Bio-Design and Manufacturing (2024) 7:1018–1034
https://doi.org/10.1007/s42242-024-00309-y

RESEARCH ARTICLE

Novel heart valve leaflet designs with stiff polymeric materials and biomimetic kinematics

Caroline C. Smid[1] · Georgios A. Pappas[1] · Nikola Cesarovic[2,3] · Volkmar Falk[2,3,4] · Paolo Ermanni[1]

Received: 12 April 2024 / Accepted: 9 July 2024 / Published online: 26 November 2024

Abstract

Despite continuous efforts to improve the robustness of cardiac valve implants, neither bioprosthetic nor mechanical valves fulfill both hemodynamic and durability requirements. This study discussed novel flexible leaflet designs, focusing on polymeric materials with proven hemocompatibility, such as polyether ether ketone, of much higher stiffness than native tissue, aiming at optimal valve implants. A biomimetic valve with a single-curvature belly-curve (B-C) was used as a reference for new design variants with a double-curvature B-C with varying radii. Soft (13.2 MPa) and stiff (2.4 GPa) leaflet materials and different thicknesses were studied using lean simulations and in vitro experiments under physiologic hemodynamic conditions. The performance was assessed using opening pressure (OP) and orifice area (OA). The latter was determined by a newly developed automatized image processing tool. Experimental trends are in agreement with simulations and demonstrated that a buckling-inspired double-curvature leaflet design significantly enhances the trileaflet valve opening behavior, which is particularly advantageous for stiffer leaflet materials. Compared to the reference, the best-performing variant showed an OP improvement of 47% and 44% based on simulations and experiments, respectively. In contrast, the achieved mean pressure differential was directly comparable to state-of-the-art bioprosthetic valves. The OA was slightly reduced for new variants but still in the satisfying range.

Caroline C. Smid and Georgios A. Pappas have contributed equally to this work.

✉ Caroline C. Smid
csmid@ethz.ch

[1] Laboratory of Composite Materials and Adaptive Structures, ETH Zürich, Leonhardstrasse 21, 8092 Zürich, Switzerland

[2] Translational Cardiovascular Technologies, ETH Zürich, Leopold-Ruzicka-Weg 4, 8093 Zürich, Switzerland

[3] Department for Cardiothoracic and Vascular Surgery, Deutsches Herzzentrum der Charité, Charité Universitätsmedizin Berlin, Augustenburger Pl. 1, 13353 Berlin, Germany

[4] German Center for Cardiovascular Research (DZHK), Partner Site Berlin, Augustenburger Pl. 1, 13353 Berlin, Germany

Graphic abstract

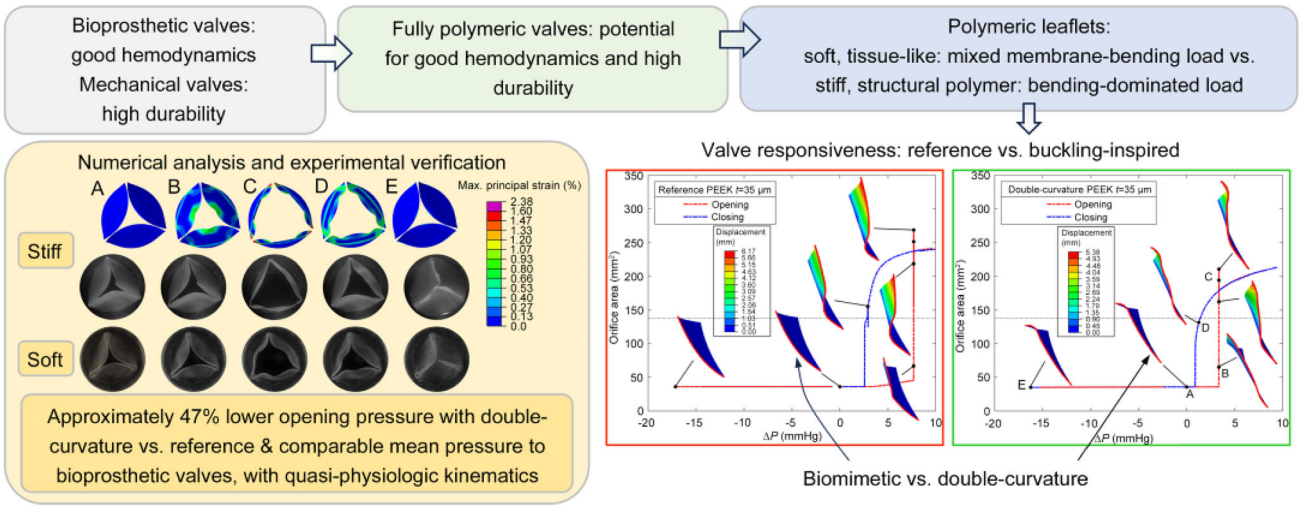

Keywords Fully polymeric heart valve · Parametric leaflet design · Finite element analysis · Leaflet kinematics · In vitro testing

Introduction

Two types of contemporary heart valves exist. Mechanical bileaflet valves made of carbon (or titanium) provide long-term durability, but also poor hemodynamics that can lead to flow cavitation [1] and therefore need lifelong anticoagulation. In contrast, bioprosthetic heart valves (BHVs) consist of leaflets made of bovine or porcine pericardium mounted on a fixed (surgical implants) or expandable (transcatheter valves) stent frame after a labor-intensive process. Although long-term anticoagulation is not required with BHVs, they are subject to leaflet degeneration, typically resulting in structural valve failure during longer-term follow-up and limiting their durability. Therefore, the lifetime management for treating valvular heart disease includes implant-related factors, such as the need for anticoagulation and durability, and patient-related factors, such as age at time-of-index operation, comorbidities, access, and patient preferences [2].

With demographic changes, the increasing demand for heart valves will surpass 850,000 annually worldwide by 2050 [3]. Given the current limitations of state-of-the-art valve technology, it is crucial to explore new valve concepts that provide improved durability without compromising the hemodynamic performance. This includes using new materials, innovative designs, and advances in manufacturing techniques. To date, no Food and Drug Administration (FDA)-approved valve has successfully combined the long-term durability typical of mechanical heart valves (MHVs) without the need for anticoagulation [4].

Considering the limitations of available materials emulating natural leaflet compliance, such as poor durability, it seems necessary to explore alternative options, including stiffer materials that could, however, result in poor hydrodynamics [5]. For instance, MHVs made of approximately 2000× stiffer materials [6] employ a two (or three) flat-disk design instead of an anatomical design, like native valves. Fully polymeric heart valves (PHVs) with robust leaflets made of strong and stiff polymeric materials pose a promising solution. These materials can be even ~300× stiffer than natural leaflet tissue [7] in terms of Young's modulus, but also of higher strength. Nevertheless, using significantly stiffer (and stronger) leaflet materials necessitates a novel valve design to achieve the requested leaflet kinematics at low pressures.

In this study, novel leaflet design concepts that may facilitate the use of stiff materials were introduced and analyzed by lean, solid mechanics-based finite element (FE) simulations and assessed by in vitro hydrodynamic experiments using a custom-built pulse duplicator (PD) [8]. The ultimate objective was to incorporate stiff material leaflets with proven hemocompatibility, such as polyether ether ketone (PEEK) [9], into a heart valve design able to approach the kinematics and hemodynamic performance of best-in-class BHVs, approaching a native valve. The motivation for the use of PEEK is high, as it shows low thrombogenicity based on animal trials conducted without antithrombotic medication [10] with a valve featuring rigid PEEK leaflets [11]. Although predominantly inert, PEEK can also support endothelialization through surface modification [12].

Background

Valve design performance assessment criteria across all prosthesis types include low transvalvular opening pressure (OP), large orifice area (OA), and tight closing. Research on flexible synthetic PHVs started almost simultaneously with durable MHVs and hemocompatible BHVs. Durability refers to the valve's ability to withstand long-term operation without significant degradation or structural failure, considering factors such as material aging, calcification, and stress-induced wear due to fatigue loading imposed during the cardiac cycle. The term hemodynamics refers to flow dynamics and performance characteristics of a heart valve within blood circulation, identified by parameters such as pressure differential (ΔP; often referred to as pressure gradient [13]) and flow characteristics, assessing flow obstruction or regurgitation [14].

Polymers offer design freedom and simple manufacturing processes. Despite design variations and materials attested, including polyurethane (PU), polytetrafluoroethylene, and silicone compounds, such PHVs initially showed insufficient biostability and poor durability [15]. Only after a big leap in material science and nanotechnology did PHVs come back into focus [14–17], with new concepts to include segmented copolymers and polymer nanocomposites [18–20]. Despite these advancements, PHVs have not been able to mimic native valve properties.

Native materials typically exhibit Young's modulus from 0.03 to 90 MPa [14, 17]. Specifically, native aortic leaflet tissue has elastic moduli of approximately 4 and 15 MPa in radial and circumferential directions, respectively [21], attributed to the circumferential orientation of collagen fibers [22]. First- and new-generation polymers generally fall within the modulus range of native materials, with some reaching 200 MPa and 4 to 100 MPa [14, 17], respectively.

Examples of currently examined PHVs from the international community are detailed in Table 1. While making notable advancements, limitations persist and there is still no FDA-approved PHV, with PHVs only commercially available in ventricular assist devices (VADs) [23]. Recognizing the essential need for noninvasive implantation and the persisting challenge of ensuring reproducible manufacturing of soft polymeric leaflets [24], a revised approach is being pursued.

Preliminary evaluation of heart valve designs has shifted from experiments [35] and animal trials [36] to advanced simulations. Solid mechanics-based simulations [28, 38–40] offer efficiency, acknowledging the simplification in boundary conditions [23], whereas fluid-level simulations mainly focus on hemodynamics [37]. Fluid–structure interaction simulations provide more accurate predictions, albeit at a much higher computational cost [23, 37], thus are often adopted at the design verification phase. Although advanced simulations hold promise for optimizing heart valve prosthesis designs, the results of such simulations depend heavily on modeling approximations. Conventional in vitro and in vivo tests are therefore vital to provide input for design iterations and modeling and validate promising designs [37].

Materials and methods

Leaflet design and conceptualization

Design benchmarking

Understanding leaflet behavior is crucial for improving valve design and performance. These leaflets experience complex transitions during opening and closing, with the sagittal leaflet cross-section, namely the belly-curve (B-C), undergoing the most significant shape transformation. Hence, this study emphasized design modifications related to the B-C shape.

The reference valve is a trileaflet aortic valve (AV) with a continuously increasing radius of curvature away from its center. Previously published literature [25, 35] was used to replicate this valve, which is based on conventional single-curvature leaflet designs (Fig. 1b), approximating native AVs (Fig. 1a). Leat and Fisher [35] altered geometry and thickness (t) to enhance the valve OP. They utilized a material approximately one order of magnitude stiffer (at low strains) than natural leaflet tissue, asserting a relationship expressed as OP $\sim \frac{Et^3}{R_i^3}$, assuming a clear bending load dominance, where R_i is the radius of curvature and E is the material's Young modulus [35]. The comparison between previously used spherical leaflets and reference valve leaflets (Fig. 1c) revealed that the latter exhibits superior OP under steady flow conditions but not in pulsatile flow scenarios.

Understanding the mechanics to create a robust design

Conventional biomimetic leaflets are expected to experience a combination of membrane and bending loads. The bending-dominated part of the response has buckling characteristics, often enabling rapid responsiveness. Examination of fundamental configurations, including flat, cylindrical, and spherical panels, with low thicknesses (Figs. 2a–2c) for enhanced deflection under low loads indicates that flat panels (Fig. 2d) demonstrate the lowest initial stiffness, requiring minimal load for deflection. However, as the applied load increases, the stiffness rises exponentially due to membrane loading, resulting in relatively limited maximum deflection. Conversely, curved panels (Fig. 2d) exhibit decreasing stiffness with load after a certain threshold [42]. Both cylindrical

Table 1 Examples of currently investigated PHVs by the international community, with key specifications

PHV model	Material and design	Key information
AorTech valve (RUA Life Sciences)	Elast-Eon (specially developed biostable PU) with stress-reducing design	First generation patented by Fisher [25]; durability of 800 million cycles [26] (exceeds minimum requirements of BHVs [27, 28])
PoliValve	Styrenic block copolymers with cylindrically shaped leaflets	Surgically implanted; in vitro performance above standard values [13] (expected durability 30 years); feasibility in short-term in vivo trial [29, 30]
Tria by Foldax	"Bio-inspired" design, biopolymer leaflets, PEEK stent, PTFE sewing ring, automated manufacturing [18]	FDA-approved early feasibility studies show promising results; minimal calcification traces in animal trials; one valve passed 670 million cycles (16 years) with minimal damage [18, 31, 32]
Lapeyre-Triflo FURTIVA	Three nonbiomimetic stiff PEEK disk-like leaflets [33]	Trileaflet valve with early closing characteristics resembling BHV, potentially eliminating long-term anticoagulation therapy; limited to surgical implantation [33, 34]

PHV: polymeric heart valve; PU: polyurethane; PEEK: polyether ether ketone; PTFE: polytetrafluoroethylene; BHV: bioprosthetic heart valve; FDA: Food and Drug Administration

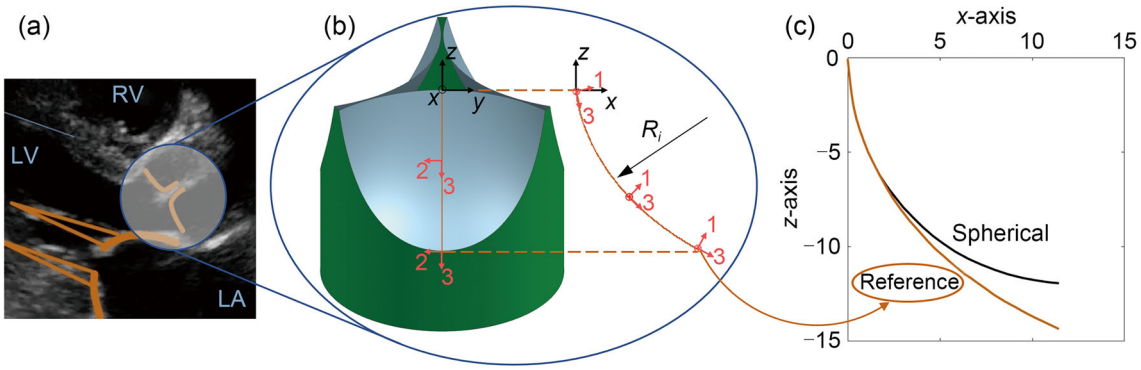

Fig. 1 **a** Echography of a native AV with B-C (in orange; reproduced from Ref. [41]; licensed under Creative Commons license). **b** Rendering of PHV 3D model based on [25, 35]. A mock continuous stent (in green) is also designed to give a better valve impression. B-C with the adopted coordinate system is also shown. **c** State-of-the-art B-C geometries (reproduced based on data in Ref. [35]). AV: aortic valve; B-C: belly-curve; PHV: polymeric heart valve

(Fig. 2b) and spherical (Fig. 2c) panels have a similar high initial stiffness but can also achieve a high maximum deflection. However, the cylindrical design presents a notable snap-through behavior with secondary stable states (Fig. 2d) [42]. Thus, an additional force is needed for recovery, potentially affecting valve closing adversely. Hence, a spherical leaflet shape shows improved deflection characteristics for the given boundary conditions.

To further elaborate on the mechanical behavior of biomimetic leaflets, sphere-shaped thin panels are simulated (PEEK material with a thickness of 50 μm; see also Sect. "Finite element analysis") with radii $R_1 = 10, 20$, and 40 mm (Figs. 2e–2g) and a constant base diameter of 10 mm and subjected to a point load at the middle with hinged edges. The trend in Fig. 2g indicates a decrease in buckling force with an increase in radius, implying that leaflet designs with large R_1 might exhibit superior performance in OP. Boundary conditions of valve leaflet have important impact on these results, but they already provide useful insights.

Designs require adaptation to accommodate materials with stiffness two to three orders of magnitude higher than natural tissue. The transition from a single-curvature B-C to a double-curvature design (Fig. 2h) is attested to further enhance the deflection tendency. Double-curvature designs resemble an imperfection, promoting buckling [43], whereas asymmetric imperfections further enhance the buckling phenomena [44]. The double-curvature design offers increased surface area across the same span, enabling greater force components in the opening direction for a given pressure.

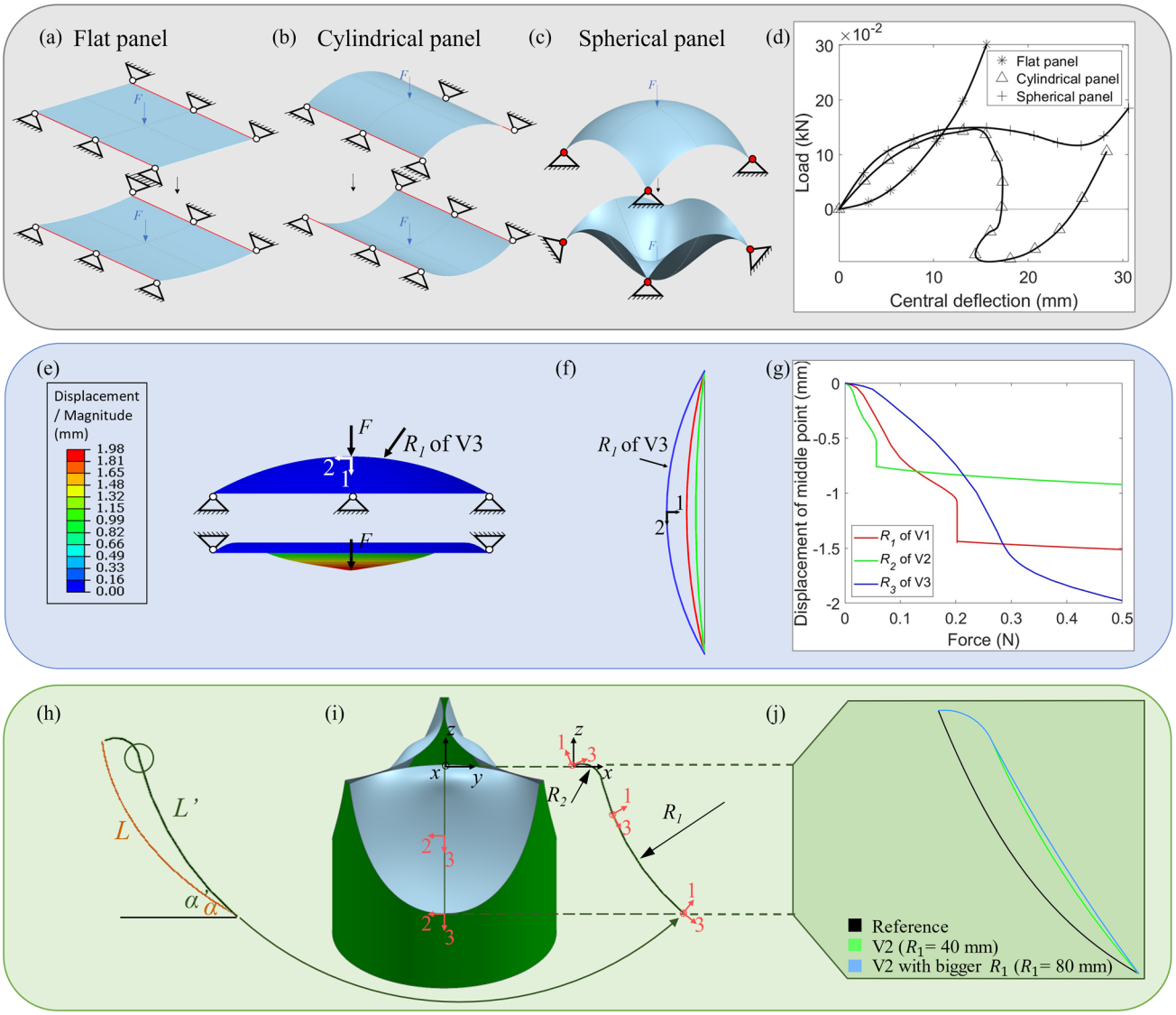

Fig. 2 **a–c** Schematics, not to scale, of basic panel geometries hinged along red edges and corners: flat, cylindrical, and spherical. **d** Their deflection upon central load (reproduced from data in Ref. [42]). **e** Simulation of the spherical panel with hinged edges and applied point load in the middle, conducted for: **f** three different leaflet radii. **g** Displacement of the middle point over the point load. **h** Geometrical differences between single and double curvature (see Table 2). **i** 3D valve model and its B-C with a coordinate system for V5. **j** Alternative, potentially more optimal, B-C shape. B-C: belly-curve

In this study, a B-C with double curvature was adopted and studied in a parametric manner by varying radii R_1 and R_2 (see Fig. 2i), resulting in five variants, as illustrated in Table 2. Valve diameter, shape of OA in the stress-free state, and stent base geometry were kept alike (see also Sect. "Finite element analysis"). Valve leaflets [25, 35] were designed (NX 12.0; Siemens Industry Software, Inc., Plano, TX, USA) in a semiopen position, with an initial OA of approximately 36 mm^2 (stress-free state), with a valve inner diameter of 22 mm (nominal OA = 380 mm^2). The starting point of R_2 coincides with the end point of R_1, resulting in a steeper inclination of the B-C due to geometrical boundary conditions (Fig. 2h).

Materials

Leaflets made of conventional soft PU (Carbothane™ PC-3585A) were considered for referencing and compared to stiff PEEK foil-based ones. All relevant information is explained hereafter.

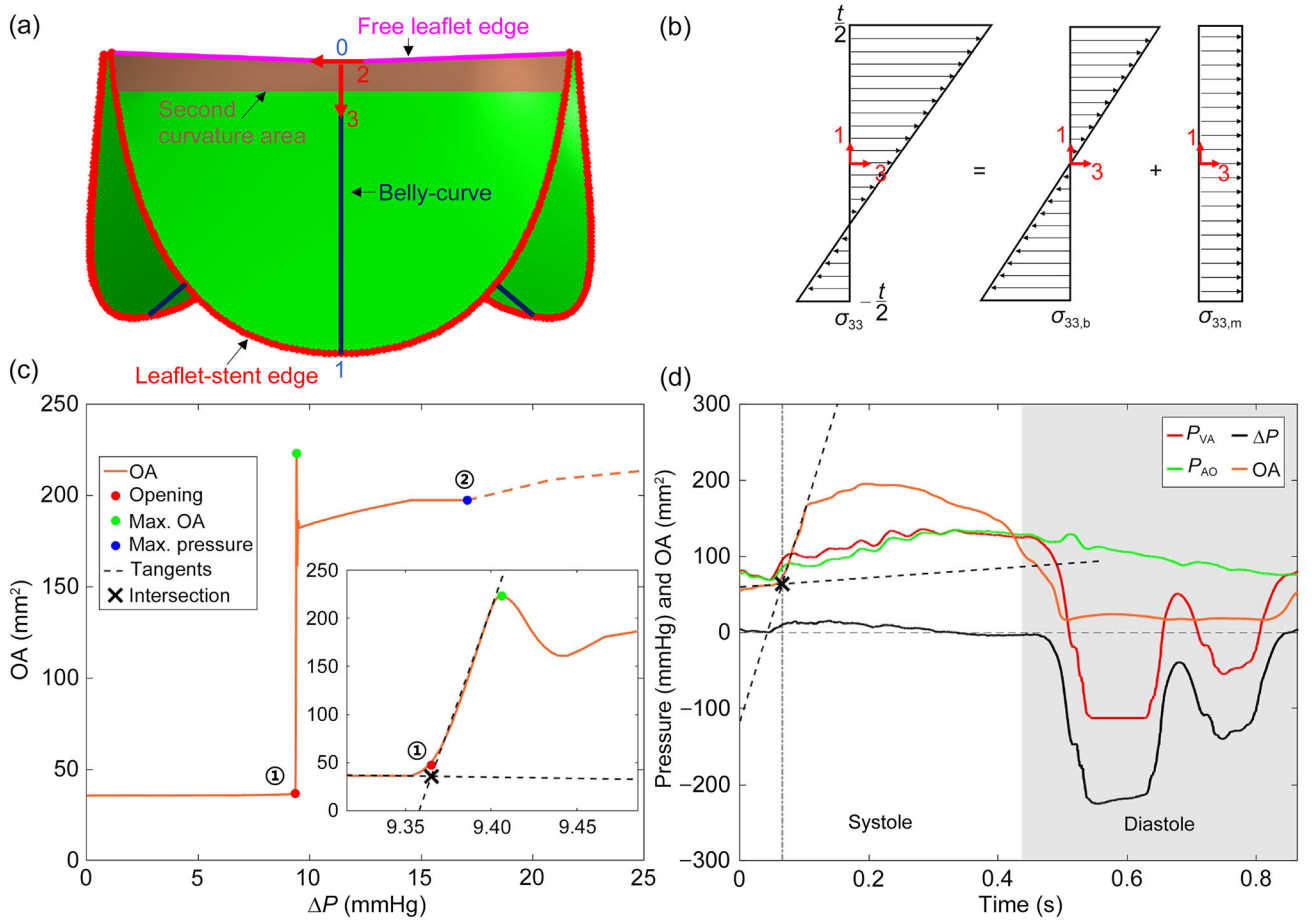

Fig. 3 **a** Leaflets with their boundary conditions and directions 2 and 3. **b** Schematic of superposition principal for stress/strain calculation. **c** Numerical OA over ΔP of V2 (PEEK, $t = 50$ μm) with tangents to determine the opening point ①, maximum OA, and maximum pressure ②. **d** Experimental pressure and OA of V2 (PEEK, $t = 50$ μm) with opening point. PEEK: polyether ether ketone

Table 2 Radii R_1 and R_2 for each variant (in mm) and cross-sections of belly-curve (B-C)

	Reference	V1	V2	V3	V4	V5
R_1 or R_{max} (mm)	56	20	40	10	20	20
R_2 or R_{min} (mm)	15.3	2.3	2.3	2.3	3	1.6
	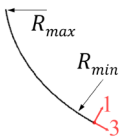	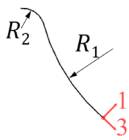	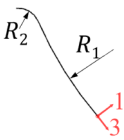	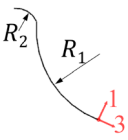	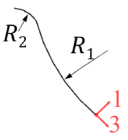	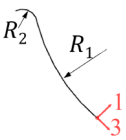

Finite element analysis

The surface models of the six valves were imported into ABAQUS version 6.14 (Dassault Systèmes, France) to conduct a quasi-static, implicit analysis. Shell elements (S4R) with quad-structured mesh from 20,000 to 24,000 and a 0.2 mm edge were chosen after an OA-OP response convergence study. Given the potential instabilities (or multistabilities), one might consider to use the Riks method [45, 46]. Nevertheless, given the involved leaflet contacts, a Newton-based solver was chosen [47] while taking care of the increment size to be sufficiently fine, as this is expected to increase the reliability of the simulations. The increment size was attested by OA-OP response convergence. Only

leaflets were modeled, and the stent was approximated as fully rigid by fixed boundary conditions along the leaflet-stent edge (Fig. 3a). A rigid stent was assumed to isolate the leaflet geometry effect but neglected the potential stent flexibility. Hard contact interaction was included to prevent interleaflet penetration, assuming a shear friction coefficient of 0.3 [38] and 0.4 [48] for PU and PEEK, respectively. A symmetry boundary condition along B-C (Fig. 3a) prevented leaflet twists related to master–slave surface contact definition in-between adjacent leaflets.

With the opening in focus, a uniformly distributed pressure was applied on the ventricular surface of the leaflet, imposing a linear increase up to the indicative 50 mmHg (1 mmHg = 133 Pa) to model ΔP. Although the experimental ΔP of the investigated valves never exceeded 33 mmHg, 50 mmHg was employed in the numerical analysis to ensure valve opening, especially for thicker and consequently stiffer leaflets. Furthermore, to capture the full kinematic behavior (i.e., valve opening and closing), a pressure history of [0, 10, 0, −20, 0] mmHg (i.e., one cycle: systole, diastole) was applied, whereas the boundary conditions stayed the same. Note that the OP for this last assay corresponded to a high level of physiologic pressure [49, 50]. In a previous study [8], this range was also confirmed for BHV, with pressure increasing from approximately 0 to 10 mmHg during leaflet separation to full opening (see Supplementary Information, Section S1).

PU and PEEK were modeled as linear elastic materials with a Young's modulus (E) of 13.2 and 2400 MPa (expected between 1900 and 3300 MPa depending on crystallinity [9, 51]) and a Poisson's ratio of 0.48 [52, 53] and 0.4 [54], respectively. PU tensile strain at break reached 450% [55], indicating its hyperplastic behavior. Nevertheless, PU was still modeled as an elastic material, as recorded strains were <12%, rendering hyperplastic modeling redundant. Young's modulus was evaluated based on the reported shore hardness [56, 57]. Leaflet thicknesses (t) of 150 [35] and 300 μm were investigated for PU. According to the first-order approximation by Leat and Fisher [35], PEEK leaflets, i.e., OP $\sim Et^3$ (for a given curvature), for PU leaflets with t = 150 μm PEEK, should have a thickness of t = 26.5 μm; this value was considered along with 35, 50, and 75 μm.

To assess the load state details, the bending and membrane strain energy ratio was calculated for soft and stiff material leaflets for the most promising design at opening (①) and maximum pressure (②) instants (Fig. 3c). Instant ② was selected near the experimental maximum ΔP of PEEK leaflets. Element volume was extracted for the two element rows along B-C and stress components, σ_{22} and σ_{33}, as a function of shell thickness . The membrane stresses (σ_{ii}^{m}) were computed based on the superposition principle (Fig. 3b) as follows:

$$\sigma_{ii}^{\mathrm{m}} = \frac{(\sigma_{ii})_{\mathrm{top}} + (\sigma_{ii})_{\mathrm{bottom}}}{2}, \tag{1}$$

where the subscripts "top" and "bottom" refer to $\frac{t}{2}$ and $-\frac{t}{2}$ respectively. The bending slope and consequently the curvature κ_{ii} were calculated as follows:

$$\kappa_{ii} \cdot E = \frac{(\sigma_{ii})_{\mathrm{top}} - (\sigma_{ii})_{\mathrm{bottom}}}{t}. \tag{2}$$

Next, the bending strain energy (U_{b}) was calculated as follows:

$$\begin{aligned} U_{\mathrm{b}} &= \int_V \frac{1}{2}\sigma\varepsilon \mathrm{d}V = \int_{-\frac{t}{2}}^{\frac{t}{2}} \frac{1}{2}\frac{\sigma^2}{E} A \mathrm{d}y \\ &= \int_{-\frac{t}{2}}^{\frac{t}{2}} \frac{1}{2}\frac{(\kappa E t)^2}{E} A \mathrm{d}y = \frac{1}{2}\frac{\kappa^2 E t^3}{12} A, \end{aligned} \tag{3}$$

where ε and A are the strain and cross-sectional area, respectively. The membrane strain energy (U_{m}), based on the membrane stress, was calculated similarly:

$$U_{\mathrm{m}} = \int_{-\frac{t}{2}}^{\frac{t}{2}} \frac{1}{2}\frac{(\sigma_{ii}^{\mathrm{m}})^2}{E} A \mathrm{d}t = \frac{1}{2}\frac{(\sigma_{ii}^{\mathrm{m}})^2}{E} A. \tag{4}$$

The bending strain energy ratio (ψ) over the total strain energy along B-C was defined as

$$\psi = \frac{U_{\mathrm{b}}}{U_{\mathrm{b}} + U_{\mathrm{m}}}. \tag{5}$$

The nodal coordinates from every increment are loaded into an in-house MATLAB script to calculate the geometrical OA. The script creates a bounding area from the coordinates for each step, plotting the projected OA over ΔP. The opening point is the intersection between the flat closed part (as pressure builds up) and the steep opening phase (Figs. 3c and 3d). The maximum OA is evaluated right after the valve opening (typical curve shown in Fig. 3c), as pressure continuous to increase, without any meaningful flow equivalent given the quasi-static simulation. Under typical physiologic flow conditions, a ΔP drop after the valve full opening is expected (as also shown in Fig. 3d).

Experimental assessment

Valve fabrication

A 3D-printed polymer mold (Therma 289, DWS, Thiene, Italy) with a mounted stent of equivalent material was dip-coated into a 0.2 g/mL PU /N,N-dimethylacetamide solution, targeting a thickness of 150 μm [25]. PEEK leaflets were manufactured by vacuum forming a PEEK foil (Victrex APTIV® 2000, Lancashire, UK) using the equipment in [51] onto an aluminum mold with alike 3D-printed stents, with the foil subsequently being glued (Scotch-Weld-2216-B/A-Gray) to the stent (Fig. 4). At very low leaflet thickness, the material becomes fragile, particularly under membrane loads during manipulation (in view of implantation). Successful valve prototypes were produced with a 50 μm PEEK foil, highlighting the importance of a responsive valve design at this thickness despite the evident rise in bending stiffness. Note that the membrane load limit is directly proportional to the leaflet thickness.

The PHVs mentioned above were also compared to a BHV (Edwards INTUITY; inner diameter 21 mm, Edwards Lifesciences, Irvine, CA, USA) and an MHV (Medtronic Advantage; outer diameter 27 mm and inner diameter 23 mm).

Pulse duplicator set-up

The experiments were performed with a PD as described previously [8] (Fig. 4). A brief mention was made here for completeness. The AV models were placed in a compliant 3D-printed aortic root model (Elastic 50A Resin; Formlabs, Somerville, MA, USA) [58] between the outlet of the pulsatile pump (ViVitro Systems, Inc., Victoria, Canada; representing the left ventricle) and a compliance chamber (mimicking aortic and systemic compliance). The pump inlet and reservoir (representing the left atrium) were separated by a BHV (Edwards INTUITY; 21 mm) acting as a mitral valve. Distilled water circulates at room temperature ((21 ± 2) °C). The pulsatile pump created a sinusoidal flow with adjustable amplitude and frequency, maintaining a systolic/diastolic ratio of 1/2. The piston position [$\Delta(t)$] defined the imposed volume rate ($\dot{V}$) and heartbeat.

Valve behavior evaluation encompassed flow measurements, high-fidelity pressure data, and real-time imaging using a high-speed camera. All acquired data are analyzed using an in-house MATLAB script, with device output signals recorded by a microcontroller board equipped with a 12-bit analog-to-digital converter (ADC; Arduino Due). The aortic flow rate (Q_{AV}) upstream of the AV was measured with a flow sensor (SONOTEC GmbH, Halle (Saale), Germany), with an accuracy of ±100 mL/min for 0 to 5 L/min. The actual cardiac output (CO; L/min) and regurgitation were determined based on instant Q_{AV} data.

Two hydrostatic pressure sensors (Sensata Technologies, Attleboro, MA, USA) were positioned about 80 mm upstream and downstream of the AV measuring the ventricular-aortic (P_{VA}) and aortic (P_{AO}) pressure, respectively. Pressure was measured from 0 to 375 mmHg (zero reference in atmosphere) with a fidelity (linearity and hysteresis) of at least 0.025% of the full range, matching the ADC system resolution of 0.9 mmHg. $\Delta P(t)$ was evaluated over a full cycle and calculated as

$$\Delta P(t) = P_{VA}(t) - P_{AO}(t). \tag{6}$$

The mean ΔP ($\overline{\Delta P}$) is the average $\Delta P(t)$ per cycle, keeping only positive values [13].

A laparoscopic endoscope (Hopkins II, Karl Storz, Tuttlingen, Germany) was inserted downstream into a 45° Y-fitting, laying coaxial to the AV, and the valve motion was recorded with a high-speed camera (FASTCAM Mini UX100; Photron USA, Inc., San Diego, CA, USA, and MeVis-C 1.6/35 macro lens, LINOS, Göttingen, Germany), positioned directly on the endoscope at 250 frames/s and 1280 px × 1024 px resolution. A light source illuminated the heart valve. Trigger and image-capture events were fed to the ADC (fidelity of 125 μs) for synchronized data acquisition. Concurrently, pressure, flow, and piston-position data were recorded with a sampling rate of ~3 kHz. Final reported values were averaged over 10 consecutive cycles. Each valve was evaluated under normotensive pressure hemodynamic conditions (120/80 mmHg) at a heart rate of 70 beats/min and a CO of 5 L/min following ISO5840-3 [13]. The compliance chamber and flow restrictor were adjusted accordingly.

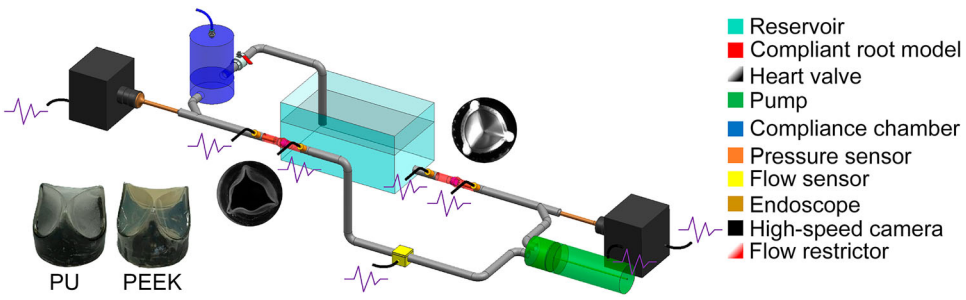

Fig. 4 Schematic of PD (see also [8]) and investigated PU and PEEK valves. PD: pulse duplicator; PU: polyurethane; PEEK: polyether ether ketone

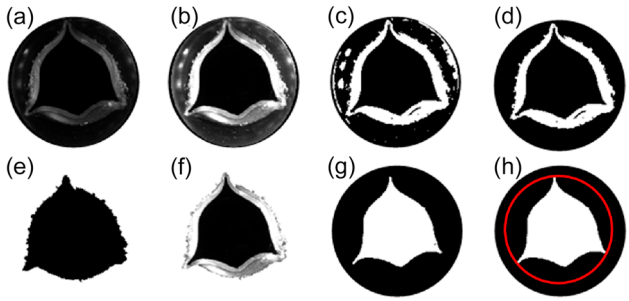

Fig. 5 OA tracking steps: **a** initial image, grayscale (8-bit); **b** image with enhanced contrast; **c** binarized image of (b); **d** largest object isolation; **e** created mask from image (d); **f** cropped image (b) with a mask; **g** largest binarized object in (f); **h** final image with artifacts corrected (see text for details). The red circle indicates the valve cylindrical stent base. OA: orifice area

Orifice area tracking

Recently, researchers [33, 59] applied efforts to track the OA using optical/pure imaging techniques. Nevertheless, given the objective of this study on evaluating alternative valve concepts, a more versatile and valve invariant technique had to be developed in a MATLAB 2022a environment, leading to an automatized image processing tool. The process intermediate results are depicted in Fig. 5. First, contrast was enhanced to highlight leaflet domains for subsequent binarization (Fig. 5b). Then, valve leaflet roots were tracked (Figs. 5c and 5d) and used as a mask to isolate the outer dark area (Fig. 5e). This led to a distinct tracking of the OA (in black in Fig. 5f). Finally, artifacts, like air bubbles, were suppressed (Figs. 5g and 5h), and the pixel sum was calculated. To correlate pixel size (in mm), a white reference circle of known diameter was positioned and imaged upfront the heart valve before starting any trial.

Results and discussion

Numerical analysis

PU and PEEK leaflets were simulated for alike flexural stiffness Et^3 to assess the validity of the first-order approximation (OP$\sim Et^3$) by Leat and Fisher [35]. Results in Fig. 6a do not support this initial hypothesis. The OPs for PEEK leaflets were up to 2.5× higher than PU, suggesting that bending-dominated load assumption is weak and insufficient for design scaling, as demonstrated in Fig. 6b, where PU (t = 150 and 300 μm; solid lines) and PEEK (t = 26.5, 35, 50, and 75 μm; dashed lines) do not follow the same path. Generally, PU has lower OPs than PEEK, attributed to the neglected membrane contribution, as explained in Sect. "Bending and membrane states".

Valve designs

The numerical analysis highlights a distinct trend in valve responsiveness, as summarized in Section "Experimental analysis". Generally, the new designs exhibited significantly lower OPs than the reference, especially with stiff leaflet materials. V2 had the lowest OP, measuring 1.1 and 9.4 mmHg for PU (t = 150 μm) and PEEK (t = 50 μm), respectively. This design provided the most significant improvement for PEEK (t = 35 μm), where OP was reduced by 56% compared to the reference, with the equivalent for t = 50 μm to be 47%. PU-based comparison still showed equivalent improvement with 37% for t = 150 μm and 55% for t = 300 μm, with a thicker leaflet to benefit more for this case. In contrast, V3 showed the lowest responsiveness, with an OP ~20% lower than the reference for PEEK (t = 50 μm). The numerical ΔP–OA paths of depictive variants can be found in Supplementary Information Section S1.

Overall, these results suggested that the double curvature leads to a higher leaflet responsiveness, based on OP, attributed to a reduced effective flexural stiffness. A large R_1 and a small R_2 favor lower OP. It appears that R_1 has a greater influence on reducing OP, as evidenced by the superior performance of V2 with a larger R_1 compared to V5 with a smaller R_2. Furthermore, the influence of R_2 on the OP becomes significant only below a certain value, as indicated by the similar performance of V1 and V4. A slight reduction in OA for the new designs is noticeable, although all exceeded the range of 138 mm^2, as reported in the norm [13], for the given nominal diameter (i.e., 22 mm). V5 had the smallest OA, up to 26% smaller than the reference design. This discrepancy may be attributed to the smallest R_2 of V5, limiting its ability to open as widely as illustrated in Supplementary Information.

Opening and closing behavior

Figure 7 illustrates noticeable differences in the opening and closing OA trajectories for the reference design and V2 for soft and stiff leaflet materials (see Supplementary Information Section S2 for other variants). The abrupt leaflet response relates to instabilities seen through the snap-through of the shell structure. During valve opening and closing, leaflet curvature changes, a phenomenon previously reported by other researchers and common in aortic leaflets [60]. An "apparent hysteresis" is observed, namely, closing occurring at lower pressures than opening. PU leaflets tend to stretch more under high pressures, whereas PEEK leaflets exhibit more diverse curvature patterns driven by bending instabilities (see Video S1 in Supplementary Information), which is apparently leading to states with higher stiffness.

This latter phenomenon is intensified for t = 50 μm, which exhibits a greater disparity in opening and closing

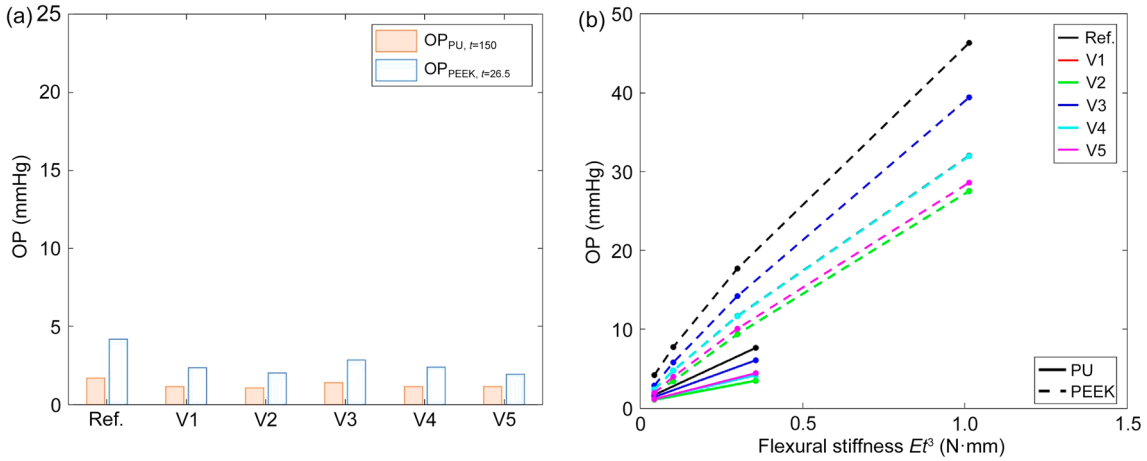

Fig. 6 OP for designs considered for **a** constant Et^3 for PU (t = 150 μm) and PEEK (t = 26.5 μm) and **b** varying Et^3 for PU (t = 150 and 300 μm; solid lines) and PEEK (t = 26.5, 35, 50, and 75 μm; dashed lines). Note the difference in the OP scale. OP: opening pressure; PU: polyurethane; PEEK: polyether ether ketone

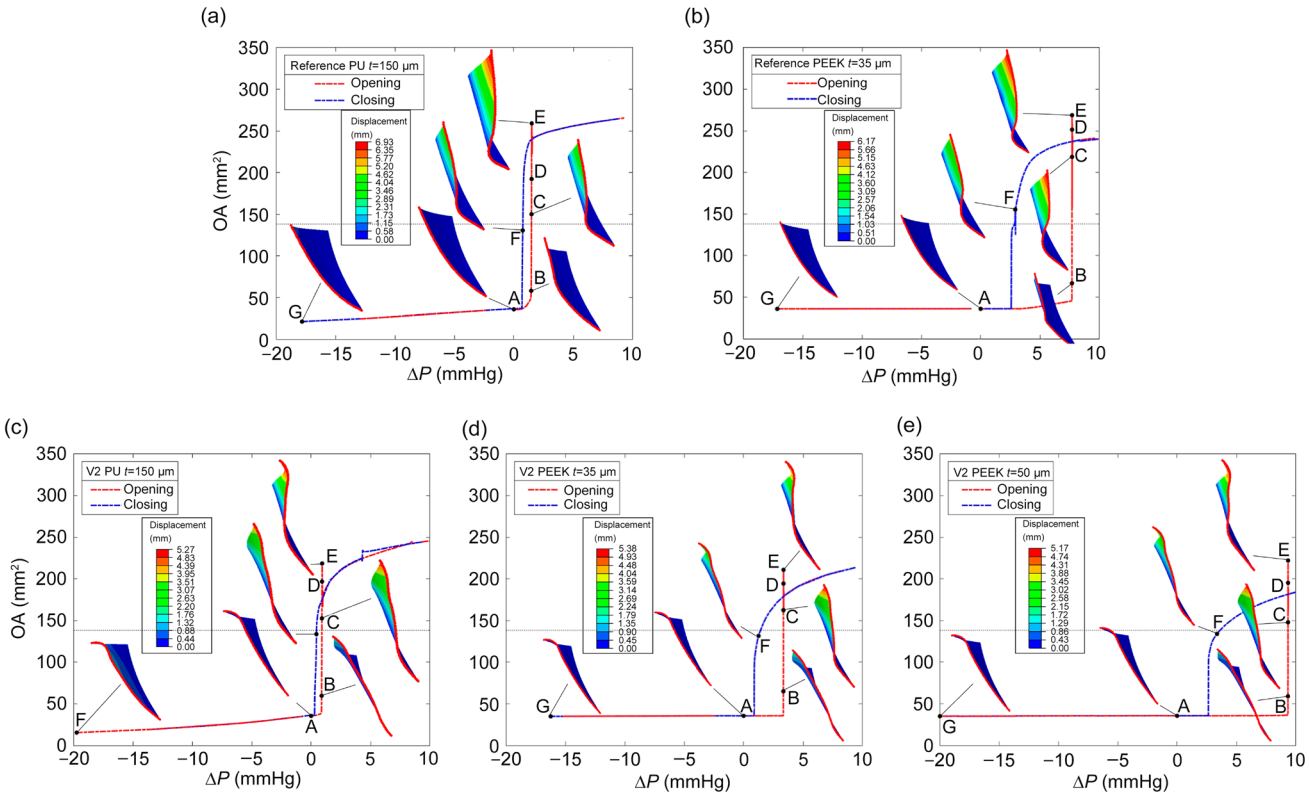

Fig. 7 Simulated OA for one cycle (systole-diastole) over ΔP for reference valve: **a** PU (t = 150 μm) and **b** PEEK (t = 35 μm) and V2: **c** PU (t = 150 μm), **d** PEEK (t = 35 μm), and **e** PEEK (t = 50 μm). The dotted line is the standard value for OA for a valve size shown in [13]. Section views of key states (see also Fig. 8) are also illustrated, with B-C marked in red and displacement magnitude in mm. Data from other variants are reported in Supplementary Information. OA: orifice area; PU: polyurethane; PEEK: polyether ether ketone; B-C: belly-curve

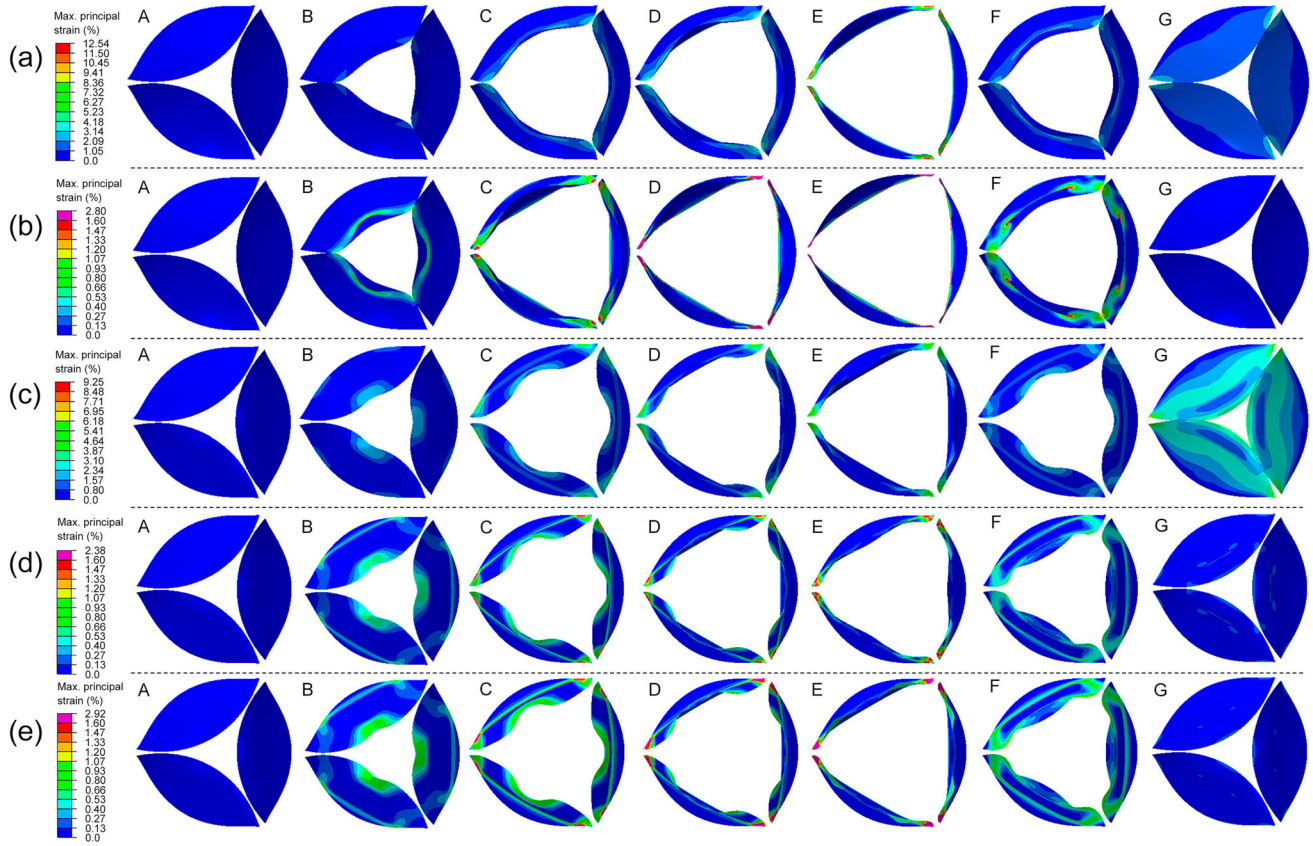

Fig. 8 Top view of opening and closing with the maximum principal strain for the instants in Fig. 7: **a** reference valve (PU, $t = 150\ \mu m$), **b** reference valve (PEEK, $t = 35\ \mu m$), **c** V2 (PU, $t = 150\ \mu m$), **d** V2 (PEEK, $t = 35\ \mu m$), and **e** V2 (PEEK, $t = 50\ \mu m$). For PEEK, elements exceeding a conservative yield limit of 1.6% [51] are shown in purple. PU: polyurethane; PEEK: polyether ether ketone

paths. Note that the complete closing of the valve is not modeled (i.e., higher negative pressures), as tight closing is weakly affected by the design variation, as shown by the experiments (see Sect. "Experimental analysis"), given the alike stress-free OA.

At the same instant, PU underwent a maximum logarithmic strain (ε_{max}) of ~12%, way below the tensile strain at break (i.e., 450%). In contrast, PEEK experienced a lower ε_{max} of ~3.5%. The latter exceeded the elastic limit, expected from 1.8% to 3% [9], but as illustrated in Fig. 8, ε_{max} is concentrated along the stent edge toward the stent tips, relating to the fixed boundary conditions. Introducing a valve frame with a certain flexibility may not alter the location of ε_{max}, but the value is expected to decrease.

Bending and membrane states

Figure 9 shows the bending and membrane stresses (σ_{22} and σ_{33}) along the normalized length (ranging from the free edge to the fixed boundary, i.e., from 0 to 1, as in Fig. 3a) of the leaflet B-C for the opening and maximum pressure (defined as in Fig. 3c), including V2 in PU ($t =$ 150 μm) and PEEK ($t = 50\ \mu m$). The stress comparison revealed a significant difference in magnitude, with PEEK ($\sigma_{max} \approx 8.0$ MPa, $\varepsilon_{max} \approx 0.33\%$) exhibiting higher stress levels than PU ($\sigma_{max} \approx 0.19$ MPa, $\varepsilon_{max} \approx 1.4\%$) at maximum pressure, relating to material moduli and load case, with maximum stresses lying in direction 2.

The calculated strain energy ratio (ψ) between bending and total strain energy (including σ_{22} and σ_{33}; Figs. 9e, 9f, 9k, and 9l), was 0.82 and 0.87 at the opening and 0.72 and 0.85 at maximum pressure for PU and PEEK, respectively, suggesting a bending-dominated problem in both cases but more pronounced in PEEK attributed to its higher stiffness. Moreover, bending stresses in direction 3 and strain energy were higher (especially) for PEEK than those in direction 2, demonstrating the importance of the B-C shape. Indicatively, the ratios of bending strain energy in direction 3, over total at the opened state shown were 0.55 and 0.71 for PU and PEEK, respectively.

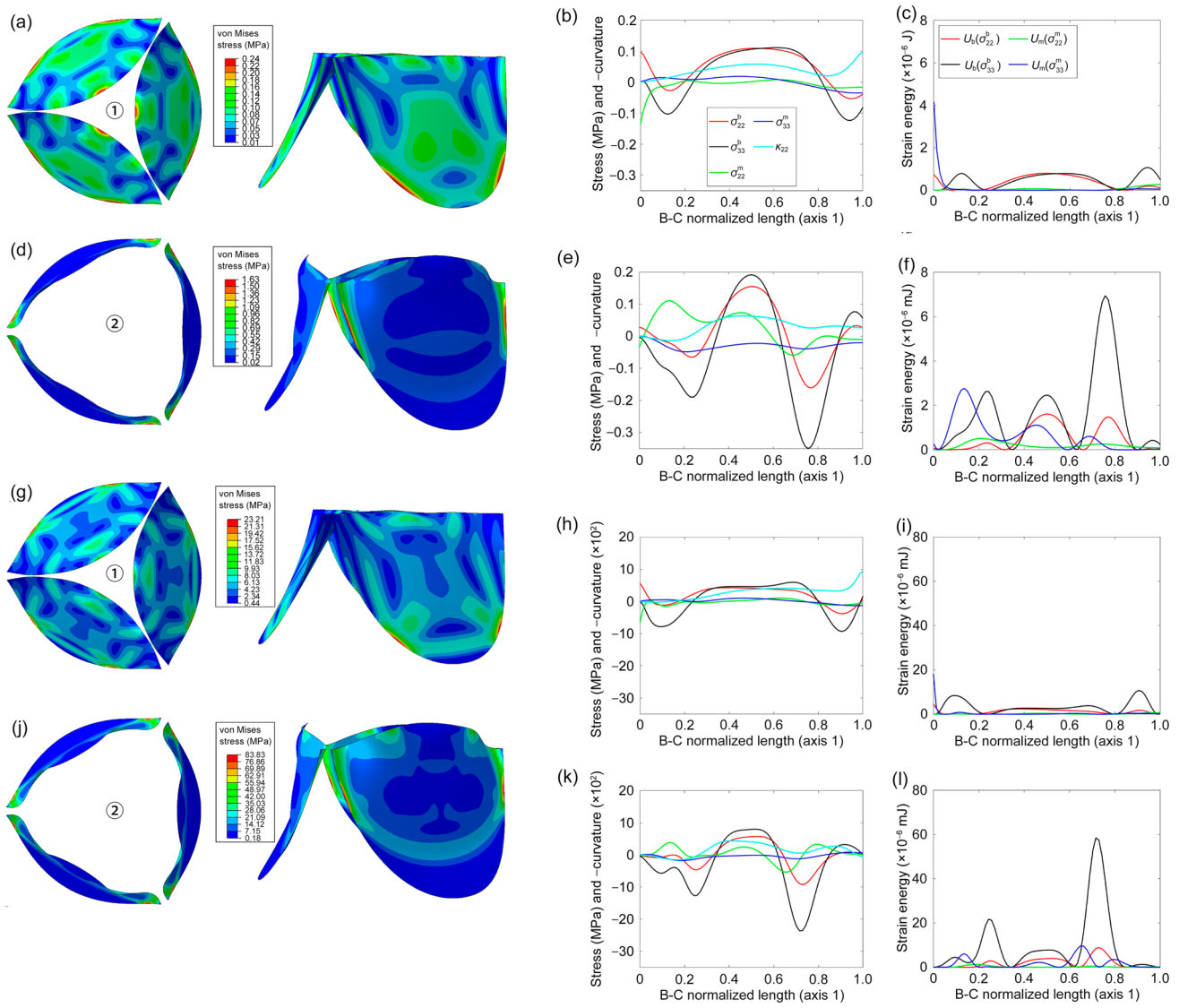

Fig. 9 Deformed state information of V2 at opening instant ① (see Fig. 3c) and maximum pressure defined at instant ② (see Fig. 3c; approximately 17 mmHg) for PU ($t = 150$ μm; (**a**–**f**)) vs. PEEK ($t = 50$ μm; (**g**–**l**)). From left to right: deformed states with von Mises stresses of V2 (**a**, **d**, **g**, **j**); bending (at $t/2$ in Fig. 3) and membrane stresses around directions 2 and 3 and curvature κ_{22} (**b**, **e**, **h**, **k**); and bending and membrane strain energy around directions 2 and 3 (**c**, **f**, **i**, **l**). Note the scale changes. PU: polyurethane; PEEK: polyether ether ketone

Experimental analysis

The experimental results (as summarized in Fig. 10) depict similar trends to FE simulations in OPs for PU and PEEK valves. The OPs for PEEK leaflets were lower than the simulation predictions (Fig. 10b), mainly due to their final thickness (after thermoforming from (45 ± 7) μm [51] compared to the simulated nominal 50 μm). The reference valve exhibited the highest OP (14.2 mmHg), whereas V2 demonstrated the lowest (8.0 mmHg), representing a 44% improvement. The $\Delta\overline{P}$ values (refer also to Fig. 11e) were in a physiologic range of 5.5–6.9 mmHg [61] and compared well to the state-of-the-art BHV reference (5–11 mmHg [49]). However, there was still potential for studies to improve the responsiveness, as discussed in Sect. "Discussion on shape optimality", given that BHV and MHV may demonstrate OPs as low as ~1 and ~2 mmHg, respectively (see Supplementary Information and [8]).

Despite the trend coincidence, the OPs for the PU valve were rather high compared to expectations, as explained in Supplementary Information Section S3. However, the tested PU valves inherited manufacturing imperfections in thickness, which were attributed to the dip-coating process (also in Supplementary Information). Thus, they were compared to

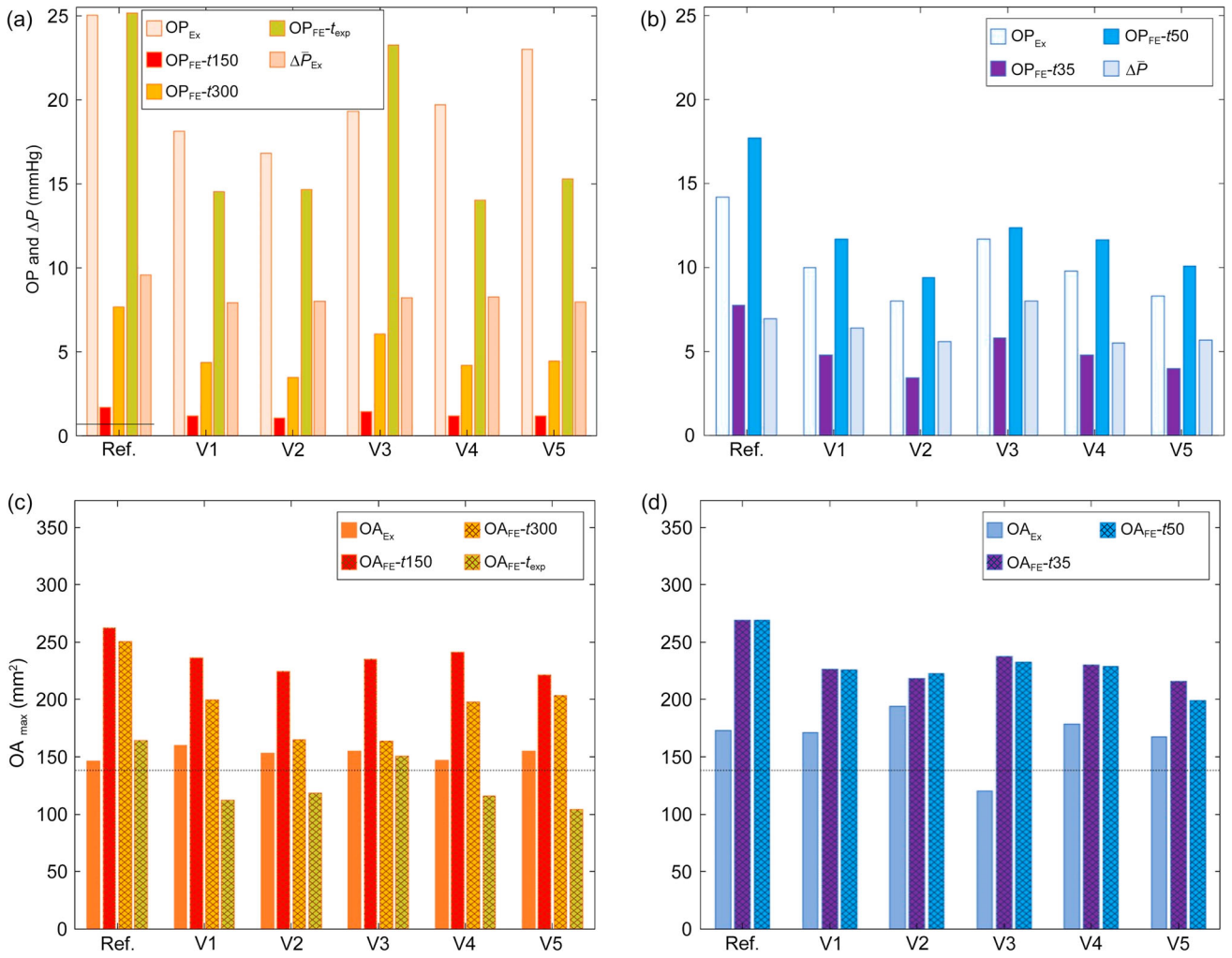

Fig. 10 Comparison of experiments with PD and FE simulations. OP and $\Delta\overline{P}$ of all designs: **a** PU and **b** PEEK. Maximum OA: **c** PU and **d** PEEK. The line in (a) is the OP of the reference valve with $E = 6$ MPa, $t = 150$ μm (see Supplementary Information). The dotted line in (c) and (d) is the standard value for OA for a valve size shown in [13]. PU: for experiments nominal $t = 250$ μm with variation explained in Supplementary Information; for simulations, t was fitted exponential thickness distribution, as described in Supplementary Information. PEEK: for experiments t=(45 ± 7) μm [51] and simulations $t = 35$ and $t = 50$ μm. PD: pulse duplicator; FE: finite element; PU: polyurethane; PEEK: polyether ether ketone; OP: opening pressure; OA: orifice area

simulation predictions by incorporating the measured thickness distribution from produced coupons; the actual mean thickness ($\bar{t}_{\text{exp}}$) along B-C was ~250 μm.

The latter simulations coincided well with the experiments. In contrast, the lower thickness (PU $t = 150$ μm) models can relate better to literature resources [35], with a perfect coincidence when the exact material properties were employed (6 vs. 13.2 MPa; see also Supplementary Information Section S1). Among the experimentally tested PU variants, the reference valve exhibited the highest OP (25 mmHg), whereas V2 showed the best OP (16.8 mmHg) with an improvement of 33%. V5 did not follow the predicted trend of being the worst PU variant, suggesting that manufacturing imperfections may have a greater influence on this particular design. $\Delta\overline{P}$ values (7.9–9.6 mmHg; see also Fig. 11e) fell within a normal to slightly elevated range [60].

OAs for PU variants exceeded the values predicted by the simulations utilizing the measured thickness distribution, whereas OAs for PEEK were lower. In most cases, the OA for PU leaflets was even less than for PEEK but mainly attributed to the resulting higher thickness (and distribution) compared to literature [35] (see also Supplementary Information). OAs remained in a satisfactory range, surpassing, for most cases, the required value (dotted line in Fig. 10) of approximately 138 mm^2 for a valve of that diameter (i.e., 22 mm), as defined by the norm [13]. This discrepancy could be attributed to slightly deviating geometry and fluid-structure interactions, such as nonuniform pressure distributions.

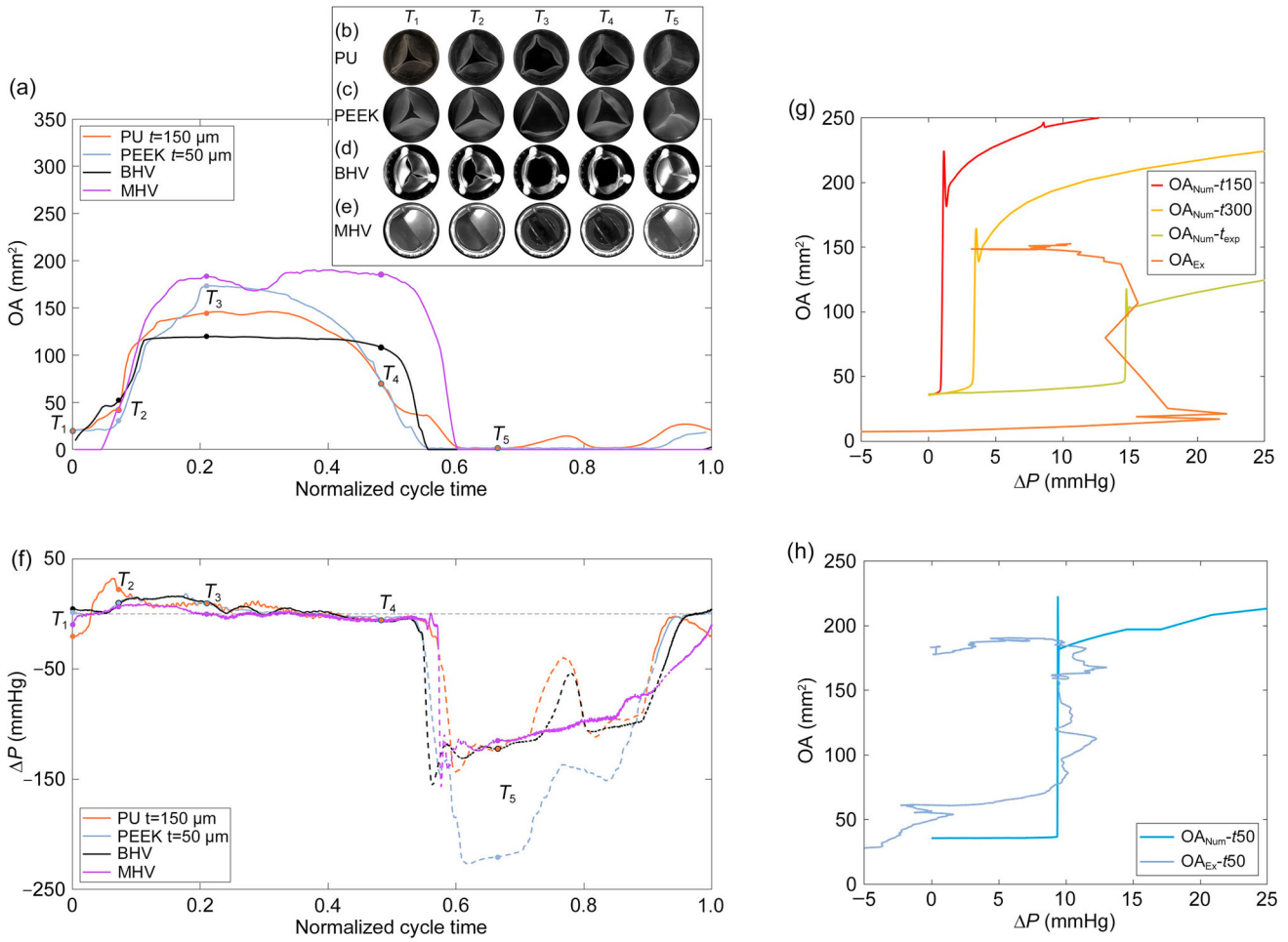

Fig. 11 Left: **a** OA plotted over normalized cycle time with key top-view snapshots of **b** reference PU ($t = 150$ μm), **c** reference PEEK ($t = 50$ μm), **d** BHV, **e** MHV, and **f** ΔP plotted over a normalized cycle time. Dashed lines contain nonindicative data out of the sensing range. Right: OA plotted over ΔP (numerical and experimental) for V2 **g** PU ($t = 150$ μm) and **h** PEEK ($t = 50$ μm). PU: polyurethane; PEEK: polyether ether ketone

In Fig. 11a, the OAs of PU and PEEK leaflets for the reference valve in the PD have similarities over a normalized cycle and, interestingly, lie between the BHV and MHV, yet, there were also a few differences between the materials. The start of the opening for PEEK leaflets occurred at a very similar instant to the PU ones (T_2). However, the pressure build-up, and consequently OP, were significantly lower for PEEK (Fig. 11e), which aligned closely with BHV. MHV exhibited even lower OP, with an OA ~1.5× larger than that of BHV. This was attributed to the inherent design of MHVs (bileaflet, hinged) and potentially its slightly larger inner diameter. At a fully opened state (T_3), the maximum OA of PEEK was greater than that of PU (see also Figs. 10c and 10d). Both valves exhibited tight closing behavior, although the PEEK leaflets closed faster. BHV closing was more abrupt, yet the fully closed state happened simultaneously with the PEEK valve. MHV also had an abrupt but delayed closing, a common characteristic for that valve type [8]. The PEEK leaflets appeared to have a small twist at full closing (T_5), attributed to the combined action of tip bending and minor inaccuracies. The PU ones with high extensibility (much lower modulus) could show tight closing without the minor twist. The recording of the opening and closing can be found in Video S1 (Supplementary Information).

Discussion on shape optimality

Having identified the effect of curve radius on the buckling force, a simulation was conducted on V2 with an increased R_1 of 80 mm (Fig. 2j). Despite the previously established trend of increased radius for a lower OP, the measured OP increased by 11% compared to V2 at a value of 10.4 mmHg. This might be attributed to the flattening of B-C as the radius increases, causing the leaflet shape to approach the flat panel form, discussed in Sect. "Understanding the mechanics to create a robust design".

This study explored a buckling-inspired shape, revealing that such shapes facilitate snap-through behavior, demonstrating potential for further investigation. Sensitivity analysis, including automatized optimization, may be the topic of further studies to explore the optimality of adopted shapes in correlation with the imposed boundary conditions. This benefit is expected to be translated on different valve sizes, but valve size shall be included in any optimization, assuming potential dependency to trigger buckled shape.

Conclusions

Having identified the lack of an idealized firm equivalent to a biological leaflet for heart valve prosthesis, this study focused on the feasibility of implementing high-grade polymers as viable solutions for artificial heart valve leaflet designs. This work demonstrated that materials with E-moduli, far exceeding that of biological tissues, have a high potential to be used for valve leaflets, provided that designs deviate from biomimetic ones. The leaflet behavior transitions from a mixed membrane-bending load state to a rather bending-dominated one during the transition from tissue-like materials (low modulus) to high-grade polymer materials (approximately 300× higher modulus). The bending dominance provides ground for the implementation of a double-curvature leaflet design (on a B-C basis), inspired by the observed buckling modes of state-of-the-art leaflets, extending the design space while resulting in a substantial improvement on the opening behavior of trileaflet valves, with particular benefit for stiffer leaflet materials. The best-performing variant shows an improvement in OP of 47% based on numerical analysis with the trends verified by the experimental in vitro hemodynamic assay (44%). This improvement places the proposed solution in direct comparison to state-of-the-art BHV prosthesis when comparing the achieved $\Delta\overline{P}$ of 5.6 vs. 9 mmHg [49].

Based on the above information, we can clearly identify and propose for the first time a very promising leaflet design that can accommodate kinematics that resembles physiologic leaflet behavior using PEEK, a material with proven hemocompatibility that includes high inertness while being one of the most mechanically performing structural polymers. Future studies should attest to the combination of material-blood interaction and offered hemodynamics to access any shear stress-related blood reaction in an in vivo environment.

The most promising design may still be subject to higher-level optimization, which can be founded on the adopted lean simulation scheme, having proven efficacy and reliability for performance assessment based on the trends identified by conducted experiments.

Supplementary Information The online version contains supplementary material available at https://doi.org/10.1007/s42242-024-00309-y.

Acknowledgements This work was partially funded by the ETHeart initiative from the Open ETH program by the Executive Board of ETH Zurich and the Zurich Heart project of Hochschulmedizin Zürich. The authors acknowledge the support of Paul Bonnet Salvador, Tim Rogenmoser, and Damaris Bartholet on preliminary pilot simulations and experiments.

Author contributions Conceptualization, CCS, GAP, NC, VF, and PE; Data curation, CCS; Formal analysis, CCS and GAP; Funding acquisition, VF and PE; Investigation, CCS and GAP; Methodology, CCS, GAP, NC, and PE; Project administration, GAP; Software, CCS and GAP; Supervision, GAP and PE; Validation, CCS, Visualization, CCS and GAP; Writing—original draft, CCS and GAP; Writing—review & editing, GAP, VF, and PE.

Funding Funding was provided by Board of the Swiss Federal Institutes of Technology and Universität Zürich and the Laboratory of Composite Materials and Adaptive structures.

Declarations

Conflict of interest The authors declare that they have no conflict of interest.

Ethical approval This study does not contain any studies with human or animal subjects performed by any of the authors.

References

1. Qian JY, Gao ZX, Hou CW et al (2019) A comprehensive review of cavitation in valves: mechanical heart valves and control valves. Bio-Des Manuf 2(2):119–136. https://doi.org/10.1007/s42242-019-00040-z
2. Windecker S, Okuno T, Unbehaun A et al (2022) Which patients with aortic stenosis should be referred to surgery rather than transcatheter aortic valve implantation? Eur Heart J 43(29):2729–2750. https://doi.org/10.1093/eurheartj/ehac105
3. Yacoub MH, Takkenberg JJM (2005) Will heart valve tissue engineering change the world? Nat Clin Pract Cardiovasc Med 2(2):60–61. https://doi.org/10.1038/ncpcardio0112
4. Marom G, Einav S (2020) New insights into valve hemodynamics. Rambam Maimonides Med J 11(2):e0014. https://doi.org/10.5041/RMMJ.10400

5. Bernacca GM, O'Connor B, Williams DF et al (2002) Hydrodynamic function of polyurethane prosthetic heart valves: influences of Young's modulus and leaflet thickness. Biomaterials 23(1):45–50. https://doi.org/10.1016/s0142-9612(01)00077-1
6. Serino G, Gusmini M, Audenino AL et al (2021) Multiscale characterization of isotropic pyrolytic carbon used for mechanical heart valve production. Processes 9(2):338. https://doi.org/10.3390/pr9020338
7. Balguid A, Rubbens MP, Mol A et al (2007) The role of collagen cross-links in biomechanical behavior of human aortic heart valve leaflets–relevance for tissue engineering. Tissue Eng 13(7):1501–1511. https://doi.org/10.1089/ten.2006.0279
8. Smid CC, Pappas GA, Falk V et al (2024) A parametric study on pulse duplicator design and valve hemodynamics. Artif Organs 48(9):977–987. https://doi.org/10.1111/aor.14757
9. Chen MJ, Pappas GA, Massella D et al (2023) Tailoring crystallinity for hemocompatible and durable PEEK cardiovascular implants. Biomater Adv 146:213288. https://doi.org/10.1016/j.bioadv.2023.213288
10. Langenaeken T, de Meester P, Verbrugghe P et al (2023) In vivo performance of a tri-leaflet mechanical heart valve prosthesis in an ovine model. Interdiscip Cardiovasc Thorac Surg 37(2):ivad142. https://doi.org/10.1093/icvts/ivad142
11. Carrel T, Vogt PR, Obrist D et al (2023) Evolving technology: the TRIFLO tri-leaflet mechanical valve without oral anticoagulation: a potential major innovation in valvesurgery. Front Cardiovasc Med 10:1220633. https://doi.org/10.3389/fcvm.2023.1220633
12. Young ER, Martin C, Ribaudo JG et al (2024) Surface modification of PEEKs with cyclicpeptides to support endothelialization and antithrombogenicity. Mater Today Commun 39:108664. https://doi.org/10.1016/j.mtcomm.2024.108664
13. International Organization for Standardization (2021) Cardiovascular implants — cardiacvalve prostheses. Part 3: heart valve substitutes implanted by transcatheter techniques. 5840–3
14. Rezvova MA, Klyshnikov KY, Gritskevich AA et al (2023) Polymeric heart valves will displace mechanical and tissue heart valves: a new era for the medical devices. Int J Mol Sci 24(4):3963. https://doi.org/10.3390/ijms24043963
15. Ghanbari H, Viatge H, Kidane AG et al (2009) Polymeric heart valves: new materials, emerging hopes. Trends Biotechnol 27(6):359–367. https://doi.org/10.1016/j.tibtech.2009.03.002
16. Kuan YH, Dasi LP, Yoganathan A et al (2011) Recent advances in polymeric heart valves research. Int J Biomater Res Eng 1(1):1–17. https://doi.org/10.4018/ijbre.2011010101
17. Oveissi F, Naficy S, Lee A et al (2020) Materials and manufacturing perspectives in engineering heart valves: a review. Mater Today Bio 5:100038. https://doi.org/10.1016/j.mtbio.2019.100038
18. Jenney C, Millson P, Grainger DW et al (2021) Assessment of a siloxane poly(urethane-urea) elastomer designed for implantable heart valve leaflets. Adv NanoBio Res 1(2):2000032. https://doi.org/10.1002/anbr.202000032
19. Rahmani B, Tzamtzis S, Sheridan R et al (2017) In vitro hydrodynamic assessment of anew transcatheter heart valve concept (the TRISKELE). J Cardiovasc Transl Res 10(2):104–115. https://doi.org/10.1007/s12265-016-9722-0
20. Ovcharenko EA, Seifalian A, Rezvova MA et al (2020) A new nanocomposite copolymer based on functionalised graphene oxide for development of heart valves. Sci Rep 10(1):5271. https://doi.org/10.1038/s41598-020-62122-8
21. Desai A, Vafaee T, Rooney P et al (2018) In vitro biomechanical and hydrodynamic characterisation of decellularised human pulmonary and aortic roots. J Mech Behav Biomed Mater 79:53–63. https://doi.org/10.1016/j.jmbbm.2017.09.019
22. Snyder Y, Jana S (2023) Trilayer anisotropic structure versus randomly oriented structure in heart valve leaflet tissue engineering. Bio-Des Manuf 6(4):423–438. https://doi.org/10.1007/s42242-023-00237-3
23. Li RL, Russ J, Paschalides C et al (2019) Mechanical considerations for polymeric heart valve development: biomechanics, materials, design and manufacturing. Biomaterials 225:119493. https://doi.org/10.1016/j.biomaterials.2019.119493
24. Life Sciences in Scottland (2020) Aortech announce heart valve development update. https://www.lifesciencesscotland.com/news/3488
25. Fisher J (1996) Artificial Heart Valve: United States Patent (USOO55OOO16A)
26. Bernacca GM, Mackay TG, Gulbransen MJ et al (1997) Polyurethane heart valve durability: effects of leaflet thickness and material. Int J Artif Organs 20(6):327–331. https://doi.org/10.1177/039139889702000606
27. International organization for standardization (2019) Cardiovascular implants — cardiac valve prostheses. Part 1: general requirements. 5840–1
28. Burriesci G, Marincola FC, Zervides C (2010) Design of a novel polymeric heart valve. J Med Eng Technol 33(1):7–22. https://doi.org/10.3109/03091900903261241
29. de Gaetano F, Serrani M, Bagnoli P et al (2015) Fluid dynamic characterization of a polymeric heart valve prototype (Poli-Valve) tested under continuous and pulsatile flow conditions. Int J Artif Organs 38(11):600–606. https://doi.org/10.5301/ijao.5000452
30. Stasiak JR, Serrani M, Biral E et al (2020) Design, development, testing at ISO standards and in vivo feasibility study of a novel polymeric heart valve prosthesis. Biomater Sci 8(16):4467–4480. https://doi.org/10.1039/d0bm00412j
31. The Business Research Company (2021) Prosthetic heart valve devices and equipment global market report 2021: COVID19 impact and recovery to 2030: Report Code -TBR519E
32. Singh SK, Kachel M, Castillero E et al (2023) Polymeric prosthetic heart valves: a reviewof current technologies and future directions. Front Cardiovasc Med 10:1137827. https://doi.org/10.3389/fcvm.2023.1137827
33. Vennemann B, Rösgen T, Heinisch PP et al (2018) Leaflet kinematics of mechanical and bioprosthetic aortic valve prostheses. ASAIO J 64(5):651–661. https://doi.org/10.1097/MAT.0000000000000687
34. Carrel T, Dembitsky WP, de Mol B et al (2020) Non-physiologic closing of bi-leaflet mechanical heart prostheses requires a new tri-leaflet valve design. Int J Cardiol 304:125–127. https://doi.org/10.1016/j.ijcard.2020.01.056
35. Leat ME, Fisher J (1994) A synthetic leaflet heart valve with improved opening characteristics. Med Eng Phys 16(6):470–476. https://doi.org/10.1016/1350-4533(94)90071-X
36. Wheatley DJ, Bernacca GM, Tolland MM et al (2001) Hydrodynamic function of a biostable polyurethane flexible heart valve after six months in sheep. Int J Artif Organs 24(2):95–101. https://doi.org/10.1177/039139880102400207
37. Zakerzadeh R, Hsu MC, Sacks MS (2017) Computational methods for the aortic heart valve and its replacements. Expert Rev Med Devices 14(11):849–866. https://doi.org/10.1080/17434440.2017.1389274
38. Pfensig S, Kaule S, Sämann M et al (2017) Assessment of heart valve performance by finite-element design studies of polymeric leaflet-structures. Curr Dir Biomed Eng 3(2):631–634. https://doi.org/10.1515/cdbme-2017-0132
39. Abbasi M, Azadani AN (2020) A geometry optimization framework for transcatheter heart valve leaflet design. J Mech Behav Biomed Mater 102:103491. https://doi.org/10.1016/j.jmbbm.2019.103491

40. Zhu GY, Ismail MB, Nakao M et al (2019) Numerical and in-vitro experimental assessment of the performance of a novel designed expanded-polytetrafluoroethylene stentless bi-leaflet valve for aortic valve replacement. PLoS ONE 14(1):e0210780. https://doi.org/10.1371/journal.pone.0210780
41. icu & echo (2017) Parasternal long axis: mitral valve. https://icuecho.com/windows/plax.php
42. Sabir AB, Djoudi MS (1995) Shallow shell finite element for the large deflection geometrically nonlinear analysis of shells and plates. Thin-Walled Struct 21(3):253–267. https://doi.org/10.1016/0263-8231(94)00005-K
43. Calladine CR (1995) Understanding imperfection-sensitivity in the buckling of thin-walled shells. Thin-Walled Struct 23(1):215–235. https://doi.org/10.1016/0263-8231(95)00013-4
44. Aimmanee S, Tichakorn K (2018) Piezoelectrically induced snap-through buckling in a buckled beam bonded with a segmented actuator. J Intell Mater Syst Struct 29(9):1862–1874. https://doi.org/10.1177/1045389X17754270
45. Mukherjee A, Ali SF, Arockiarajan A (2021) Hybrid bistable composite laminates for structural assemblies: a numerical and experimental study. Compos Struct 260:113467. https://doi.org/10.1016/j.compstruct.2020.113467
46. Lele AG (2018) An investigative study of the snap through, snap-back and the stiffness properties of a kirigami unit cell. Master Thesis of Clemson University
47. ABAQUS/Standard User's Manual (2014) Version 6.14. Dassault Systèmes Simulia Corp
48. Victrex® PEEK Film Technology. VICTREX PLCAPTIV®. https://www.professionalplastics.com/professionalplastics/content/downloads/PeekFilm.pdf
49. Johnson NP, Zelis JM, Tonino PAL et al (2018) Pressure gradient vs. flow relationships to characterize the physiology of a severely stenotic aortic valve before and after transcatheter valve implantation. Eur Heart J 39(28):2646–2655. https://doi.org/10.1093/eurheartj/ehy126
50. Adam P (2008) What is an aortic valve gradient? asks Jack. https://www.heart-valve-surgery.com/heart-surgery-blog/2008/10/05/aortic-valve-gradient/ [Accessed 19 Feb 2024]
51. Chen MJ, Pappas GA, Smid CC et al (2024) Manufacturing studies of a polymeric/composite heart valve prosthesis. Polym Compos 45(12):11076–11092. https://doi.org/10.1002/pc.28532
52. Ghaill NNA, Little EG (2008) Determination of the mechanical properties of Bionate 80A and Bionate 75D for the stress analysis of cushion form bearings. Proc Inst Mech EngH 222(5):683–694. https://doi.org/10.1243/09544119JEIM372
53. Qi HJ, Boyce MC (2005) Stress–strain behavior of thermoplastic polyurethanes. Mech Mater 37(8):817–839. https://doi.org/10.1016/j.mechmat.2004.08.001
54. Illenberger CM, Tobie T, Stahl K (2022) Damage mechanisms and tooth flank load capacity of oil-lubricated peek gears. J Appl Polym Sci 139(30):e52662. https://doi.org/10.1002/app.52662
55. Gulbulak U, Ertas A, Baturalp TB et al (2020) The effect of fundamental curves on geometric orifice and coaptation areas of polymeric heart valves. J Mech Behav Biomed Mater 112:104039. https://doi.org/10.1016/j.jmbbm.2020.104039
56. Nezarati RM, Eifert MB, Dempsey DK et al (2015) Electrospun vascular grafts with improved compliance matching to native vessels. J Biomed Mater Res B Appl Biomater 103(2):313–323. https://doi.org/10.1002/jbm.b.33201
57. Gent AN (1958) On the Relation between Indentation Hardness and Young's Modulus. Rubber Chem Technol 31:896–906. https://doi.org/10.5254/1.3542351
58. Swanson M, Clark RE (1974) Dimensions and geometric relationships of the human aortic valve as a function of pressure. Circ Res 35(6):871–882. https://doi.org/10.1161/01.RES.35.6.871
59. Stanová V, Zenses AS, Rieu R et al (2017) Effect of valve- and patient- related factors on the effective and geometric orifice areas: an in vitro study with the core valve. Comput Methods Biomech Biomed Eng 20(Sup1):195–196. https://doi.org/10.1080/10255842.2017.1382929
60. Thubrikar M (1990) The Aortic Valve. CRC Press, Boca Raton Fla, USA
61. Claiborne TE, Slepian MJ, Hossainy S et al (2012) Polymeric trileaflet prosthetic heart valves: evolution and path to clinical reality. Expert Rev Med Devices 9(6):577–594. https://doi.org/10.1586/erd.12.51